Journal of Biomechanics 46 (2013) 1351–1357

Contents lists available at SciVerse ScienceDirect

Journal of Biomechanics

journal homepage: www.elsevier.com/locate/jbiomech
www.JBiomech.com

The influence of total knee arthroplasty geometry on mid-flexion stability: An experimental and finite element study

Chadd W. Clary [a,b,c,*], Clare K. Fitzpatrick [a], Lorin P. Maletsky [b], Paul J. Rullkoetter [a]

[a] Computational Biomechanics Lab, University of Denver, Denver, CO, USA
[b] Department of Mechanical Engineering, University of Kansas, Lawrence, KS, USA
[c] DePuy Orthopedics, Warsaw, IN, USA

ARTICLE INFO

Article history:
Accepted 20 January 2013

Keywords:
Total knee replacement
Kinematics
Knee simulation
Condylar geometry

ABSTRACT

Fluoroscopic evaluation of total knee arthroplasty (TKA) has reported sudden anterior translation of the femur relative to the tibia (paradoxical anterior motion) for some cruciate-retaining designs. This motion may be tied to abrupt changes in the femoral sagittal radius of curvature characteristic of traditional TKA designs, as the geometry transitions from a large load-bearing distal radius to a smaller posterior radius which can accommodate femoral rollback. It was hypothesized that a gradually reducing radius may attenuate sudden changes in anterior–posterior motion that occur in mid-flexion with traditional discrete-radius designs. A combined experimental and computational approach was employed to test this hypothesis. A previously developed finite element (FE) model of the Kansas knee simulator (KKS), virtually implanted with multiple implant designs, was used to predict the amount of paradoxical anterior femoral slide during a simulated deep knee bend. The model predicted kinematics demonstrated that incorporating a gradually reducing radius in mid-flexion reduced the magnitude of paradoxical anterior translation between 21% and 68%, depending on the conformity of the tibial insert. Subsequently, both a dual-radius design and a modified design incorporating gradually reducing radii were tested in vitro in the KKS for verification. The model-predicted and experimentally observed kinematics exhibited good agreement, while the average experimental kinematics demonstrated an 81% reduction in anterior translation with the modified design. The FE model demonstrated sufficient sensitivity to appropriately differentiate kinematic changes due to subtle changes in implant design, and served as a useful pre-clinical design-phase tool to improve implant kinematics.

1. Introduction

Kinematic performance of total knee arthroplasty (TKA) impacts the functionality and longevity of the joint (Banks et al., 2003a; Banks and Hodge, 2004a; Harman et al., 2009). A variety of factors contribute to the kinematics of the implanted knee joint, including component type (cruciate-retaining/posterior-stabilizing, fixed-bearing/rotating platform) and conformity (low conforming devices typically allow greater relative tibiofemoral motion and increase the load-bearing requirements of the surrounding soft-tissues), surgical procedure (component alignment, soft-tissue release), ligament integrity, muscle function, and loading conditions (patient weight, activity level). Relative sliding between femoral and tibial components affects wear on the insert (Blunn et al., 1991; Harman et al., 2001). Banks et al. (2003b) reported that almost 50% of variation in maximum knee flexion may be accounted for by the anterior–posterior (A–P) position of the femur on the tibia, with an additional 1.4° of flexion achieved for each millimeter of posterior femoral translation.

Fluoroscopic evaluations of TKA kinematics have reported a sudden anterior slide of the femur relative to the tibia, frequently occurring on the medial compartment (Dennis et al., 1998). This has been referred to as "paradoxical" anterior femoral slide – motion that is opposite to the normal knee, and occurs most frequently in posterior cruciate ligament (PCL)-retaining knees (Dennis et al., 2003a, 2003b; Banks et al., 2003a; Banks and Hodge, 2004b; Delport et al., 2006). Delport et al. (2006) reported that 83% of PCL-retaining knee replacements demonstrated paradoxical anterior motion, compared to 0% of PS knee replacements. Dennis et al. (2003b) reported paradoxical anterior femoral motion in 50% and 60% of PCL-retaining knees, medially and laterally, respectively. Anterior motion of the femur on the tibia has the potential to deleteriously impact TKA outcomes in several ways; anterior positioning of the femur reduces tibiofemoral range of motion, relative tibiofemoral sliding increases the potential for

* Corresponding author at: DePuy Orthopedics, Warsaw, IN, USA. Tel.: +1 574 372 7744; fax: +1 574 372 7101.
E-mail address: cclary1@its.jnj.com (C.W. Clary).

0021-9290
http://dx.doi.org/10.1016/j.jbiomech.2013.01.025

insert wear and reduces quadriceps moment arms and efficiency (Dennis et al., 2003b; Banks et al., 2003b; Mahoney et al., 2002; Blunn et al., 1991).

TKA devices are intended to accommodate a broad flexion range, with the functional requirements of the device dependant on flexion angle. Typically, a relatively large primary distal radius is used as the principal load bearing surface during low flexion, high frequency activities, such as standing or gait, to reduce stress in the insert polyethylene. A smaller posterior radius of curvature reduces the implant conformity and enables femoral rollback with knee flexion. Traditional total knee replacement designs have accommodated these varying functional demands by utilizing multiple discrete radii to define the sagittal curvature of the femoral component (J-curve); the distal radius instantaneously shifts, at a specific flexion angle, to a smaller posterior radius. Abrupt reductions in J-curve radii cause abrupt changes in the center of rotation of the femur with respect to the tibia and abrupt reductions in tibiofemoral conformity, leading to a decrease in anterior–posterior tibiofemoral stability.

It was hypothesized in this study that paradoxical anterior femoral slide in a traditional dual radius TKA is initiated by the sudden reduction from the distal to posterior femoral radii (Fig. 1). It was also hypothesized that replacing the instantaneous radius reduction with a gradually reducing radius would attenuate the paradoxical slide, and that incorporating an abruptly increasing radius would have the opposite effect, increasing posterior translation of the femur. Finally, it was hypothesized that the kinematic changes associated with enhancement of the femoral J-Curve would be moderated by the sagittal conformity of the tibial insert, with less conforming inserts exhibiting more condylar motion.

To evaluate these hypotheses, a combined experimental and computational approach was employed building on previous work utilizing the Kansas knee simulator (KKS) (Maletsky and Hillberry, 2005). The KKS is a six-degree-of-freedom electro-hydraulic mechanical simulator used to evaluate mechanics of the knee in natural and implanted cadaveric specimens. Loads applied at the hip, ankle, and quadriceps tendon create specific loading conditions at the knee simulating dynamic activities like a deep knee bend (DKB). Prior experimental and computational work focused on the development and validation of a finite element (FE) representation of the experimental simulator (Halloran et al., 2010; Baldwin et al., 2012). In the current study, the KKS computational model was employed as an iterative design tool to predict kinematic differences due to geometric modifications of the femoral and tibial TKA articular surfaces. The experimental rig was employed for verification purposes when a series of cadaveric specimens were implanted with both a traditional TKA and a new implant system embodying the geometric enhancements studied in the model and evaluated in vitro to verify both the predictive ability of the model and the kinematic effects of the modified TKA geometry.

2. Methods

2.1. Computational modeling

A computational FE model of the KKS, developed in Abaqus/Explicit (Simulia, Providence, RI), had been previously validated against the experimental rig during gait and DKB activities, demonstrating good agreement between model-predicted and experimentally measured knee kinematics (Baldwin et al., 2012; Halloran et al., 2010). The simulator model contained a computational representation of the knee, composed of specimen-specific bony geometry and soft-tissue structures. Seven ligamentous structures stabilizing the implanted tibiofemoral joint were modeled with two-dimensional (2-D) fiber-reinforced four-noded membrane elements: the lateral collateral and popliteofibular ligaments (LCL, PFL), anterior lateral capsule (ALC), superficial medial collateral ligament (sMCL), anterior-lateral and posterior-medial bundles of the PCL (alPCL, plPCL), and medial and lateral posterior capsules. Ligament pre-tension, stiffness, and attachment sites were optimized to match internal–external (I–E) and varus–valgus (Vr–Vl) passive laxity envelope data from a previously published cadaveric experiment (Baldwin et al., 2012). Details of the ligament representation, including the mechanical properties and optimization methods, were presented in detail in Baldwin et al. (2012). The PCL mechanical properties and attachment sites were taken from the literature (Harner et al., 1995; Amis et al., 2006; Race and Amis, 1994). The extensor mechanism (patellar tendon, rectus femoris, and vastus intermedius) was represented by three-dimensional (3-D) fiber-reinforced 8-noded hexahedral continuum elements. The mechanical properties of the extensor mechanism structures were determined in isolated uniaxial analyses to match literature values (Stäubli et al., 1999). Contact was defined between the soft-tissue structures and bone and implant geometry to accommodate wrapping in deeper flexion.

To assess the relationship between implant geometry and kinematics, the computational model was virtually implanted with a parametric finite element representation of cruciate-retaining (CR) TKA components (Fig. 2) and a series of eight distinct femoral geometries were assessed. The first series of three traditional femoral geometries were intended to study the effects of the transition angle from distal to posterior radii on condylar kinematics. The three femurs were composed of dual-radius J-Curves with either a large (Femur 1), medium (Femur 2), or small (Femur 3) distal radii of curvature (Table 1). To maintain consistent A–P and S–I condylar dimensions, increasing the distal radius of curvature caused the transitions to the posterior radius to occur at earlier flexion angles. The first femur transitioned from the distal to posterior radius at 10° knee flexion and had a constant radius through the remainder of the flexion range. Likewise, the second and third femurs transitioned at 20° and 33°, respectively.

The fourth and fifth femoral geometries had the same distal and posterior radii of curvature as the third traditional femur (Femur 3), but the transition from the distal to posterior radii occurred gradually over a range of flexion instead of instantaneously at a single flexion angle. The gradually reducing radius spanned from 20° to 50° flexion for Femur 4 and from 5° to 65° flexion for Femur 5. The gradually reducing radii were defined using cubic splines that were tangent to both the distal and posterior radii at the specified transition angles. Spline parameters were chosen which maintained consistent A–P and S–I condylar dimensions. The final three femurs also incorporated a gradually reducing radius from a slightly smaller distal radius to the posterior radius over the same range as Femur 5, but at the end of the gradually reducing radius there was a sudden transition to a slightly larger posterior "braking" radius. The nomenclature "braking" radius was chosen from the hypothesis that the sudden increase in radius would arrest any anterior slide and increase femoral rollback. Femur 6 was the baseline model with a slightly smaller distal radius and a gradual reduction into the posterior radius with no brake radius. Femurs 7 and 8 utilized the same distal radius and reducing radius as Femur 6, but had brake radii of +2 mm and +4 mm, respectively.

All femurs had consistent coronal condylar geometry and trochlear geometry articulating against a medialized dome patella. Each unique femur was paired

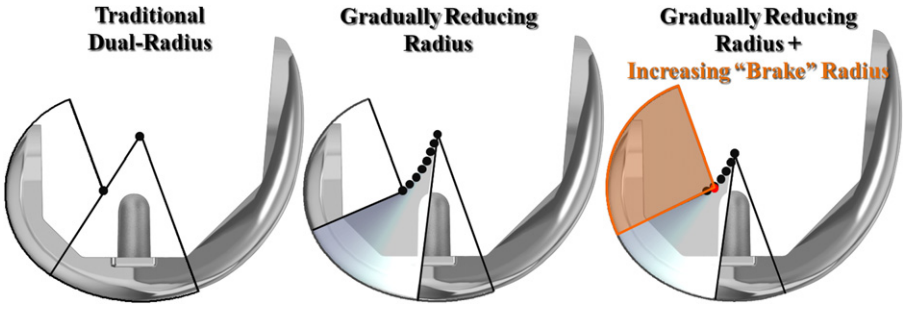

Fig. 1. Sagittal curvature of the femoral component for a traditional dual-radius design (left), for a gradually reducing radius design (center), and with a sudden increase in radius in flexion (right).

with three inserts defined by a single radius of curvature in the sagittal plane using three different conformity ratios: un-conforming (conformity ratio of distal femoral radius to insert radius=0.33), moderately conforming (ratio=0.66), and conforming (ratio=0.99). The articulating surfaces of the femurs, inserts, and patellae were meshed with rigid four-noded surface elements with 1-mm edge lengths. Previous mesh density studies verified convergence for kinematic results (Halloran et al., 2005). Contact was defined between the femur, insert and patella using a previously verified penalty-based pressure-overclosure relationship (Halloran et al., 2005). A coefficient of friction of 0.04 was applied between the metal and polyethylene articular surfaces (Godest et al., 2002; Halloran et al., 2005)

Knee kinematics for the various designs were assessed during a DKB simulation. In the KKS model, loads were applied to the knee via boundary conditions at the hip and ankle. The model allowed flexion–extension (F–E) and S–I translation at the hip, and allowed F–E, internal–external (I–E), and varus–valgus (Vr–Vl) rotations at the ankle, in addition to medial–lateral (M–L) translation. A constant 100-N hip load to simulate one-half of the body's torso weight was applied via the hip S–I axis. The compressive load applied at the hip was limited to 100-N to reduce the risk of quadriceps rupture during the cadaveric verification. The knee flexion angle during the DKB ranged from full-extension to 110°, controlled by excursion of the quadriceps tendon via a connector element fixed to the hip. The M–L translation and I–E, Vr–Vl, and F–E rotations at the ankle were unconstrained and unloaded. Local femoral and tibial coordinate systems were defined based on the implant geometry, with the origin of the femur at the center of the distal radius of curvature of the articular geometry and the origin of the tibial at the lowest point (dwell) of the insert articular geometry. Six-degree-of-freedom (6-DOF) tibio-femoral (TF) kinematics were calculated using a three-cylindrical open-chain description (Grood and Suntay, 1983). The lowest points on the femoral articular geometry along the S–I axis of the tibia were also identified. To define the magnitude of the anterior slide, the anterior–posterior (A–P) distance from the most posterior position of the medial femoral condyle prior to the radius transition to the most anterior position after the radius transition through the flexion portion of the cycle was calculated. In addition, the instantaneous helical axis of rotation between the tibia and femur was also calculated at 15° increments between 15° and 105° flexion using a 10° window around the flexion angle of interest (Woltring et al., 1985).

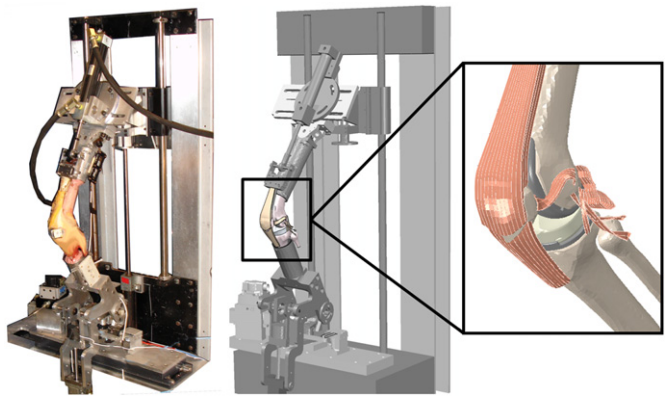

Fig. 2. Experimental Kansas knee simulator with actuators at the hip, ankle and quadriceps applying loads to the knee (left); computational representation of the experimental simulator, with loads applied in the same manner as the experiment (center); finite element model of the knee joint, including tibiofemoral soft-tissues, extensor mechanism, and TKA components (right).

2.2. Cadaveric verification

To verify the predictive abilities of the computational model, both an existing traditional dual-radius CR TKA design (PFC SIGMA knee system™, DePuy Orthopaedics, Warsaw, IN) and a modern implant system (ATTUNE knee system™, DePuy Orthopaedics, Warsaw, IN) incorporating both a gradually reducing radius (Gradius™, DePuy Orthopaedics, Warsaw, IN) and "brake" radius were evaluated in both the computational model and the experimental KKS rig. Seven fresh frozen cadaveric knees (age: 64 ± 10 years, height: 1.76 ± 0.06 m, BMI: 27.0 ± 3.8, all male, five right/two left) were implanted with the PFC Sigma knee system through a medial mid-vastus approach using standard instrumentation with ligament balancing performed at the discretion of the surgeon, and the previously described DKB simulation in the KKS was performed. Subsequently, the traditional components were removed and the Attune knee system components were implanted on the knee using the same bony preparation. Utilizing the same bone cuts ensured that implant alignment and ligament balancing were equivalent between component evaluations.

Knee motion during the DKB was measured using an Optotrak 3020 motion capture system (Northern Digital Inc., Waterloo, Ontario, Canada) with tracking arrays attached to the tibia and femur. CAD models of the knee implants were registered to probed implant locations in the tibial and femoral reference frames. 6-DOF kinematics, condylar translations, and helical axes were calculated using the same methodology described above for the computational simulations. The observed motions were averaged across the seven specimens to determine a characteristic motion, and compared with the model-predicted kinematics.

3. Results

3.1. The effect of condylar 2 radii-of-curvature on knee kinematics

Condylar translations for the traditional dual-radius femoral components (Femurs 1–3) predicted by the computational model consistently demonstrated an anterior femoral slide of the medial condyle (Fig. 3). As the traditional femurs began to flex, the rate at which the femurs rolled posteriorly correlated with the size of the distal radius; larger distal radii rolled posterior more rapidly. The rate of posterior translation was also correlated with the conformity of the tibial insert; the least conforming inserts had the most rapid posterior translation of the femur. The anterior slide initiated at the flexion angle corresponding to the instantaneous transition from the distal to posterior femoral radii-of-curvature. While the anterior slide initiated at different flexion angles, the overall magnitude of the slide was not consistently affected by the transition angle of the femoral component. However, the overall magnitude of the anterior slide was affected by the tibial conformity, with the greatest anterior slide occurring for the least conforming tibial insert. For the extension portion of the cycle, the opposite translations occurred to return the condyles to the initial position, but the paradoxical translation in mid-flexion was less distinct than in the flexion portion of the cycle. The discontinuity in the femoral radii also influenced the lateral condylar kinematics by disrupting the continuous rollback with knee flexion, but did not cause any significant anterior slide.

Replacing the instantaneous transition from the distal to posterior radius with a gradually reducing radius (Femurs 4 and 5)

Table 1
Geometric parameters of the eight different femurs evaluated in the computational model of the Kansas Knee Simulator. Femurs 1–3 have "traditional" dual-radii condylar geometries with increasing distal radii. Femurs 4–6 incorporate a gradually reducing radius instead of the instantaneous reduction in "traditional" TKA. Femurs 7 and 8 also have a gradually reducing radius, but incorporate a sudden increase in radius at 65° knee flexion.

Femur attribute	Traditional Femurs			Gradually reducing radius			Braking radius	
	Femur 1	*Femur 2*	*Femur 3*	*Femur 4*	*Femur 5*	*Femur 6*	*Femur 7*	*Femur 8*
Distal radius (mm)	46	40	34	34	34	30	30	30
Posterior radius (mm)	22	21	20	20	20	20	20	20
Transition angle (deg)	10	20	33	20–50	5–65	5–65	5–65	5–65
Condyle A–P (mm)	26	28	28	27	27	26	26	26
Condyle S–I (mm)	22	22	22	22	22	22	23	24
Brake radius (mm)	NA	NA	NA	NA	NA	NA	+2	+4

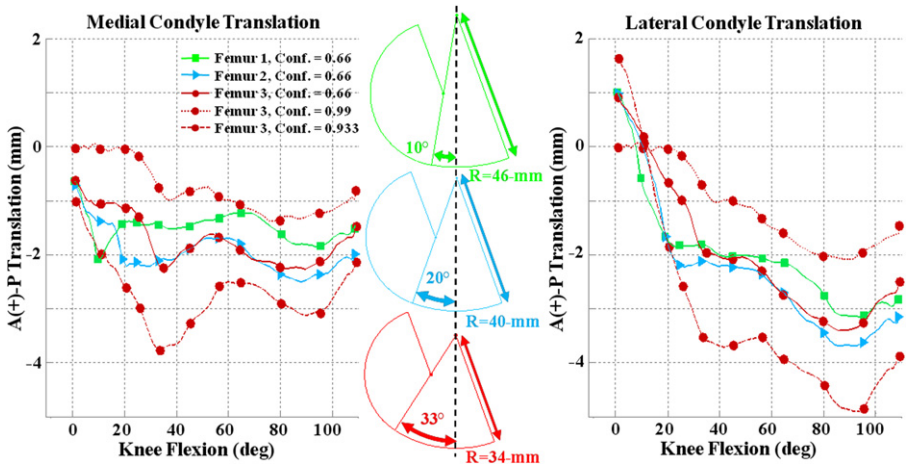

Fig. 3. Predicted A–P motion of the femoral medial condyle (left) and lateral condyle (right) for three traditional femoral components with the either a large, medium, or small distal radii-of-curvature. The femur with the small distal radii was evaluated against inserts with three conformity levels.

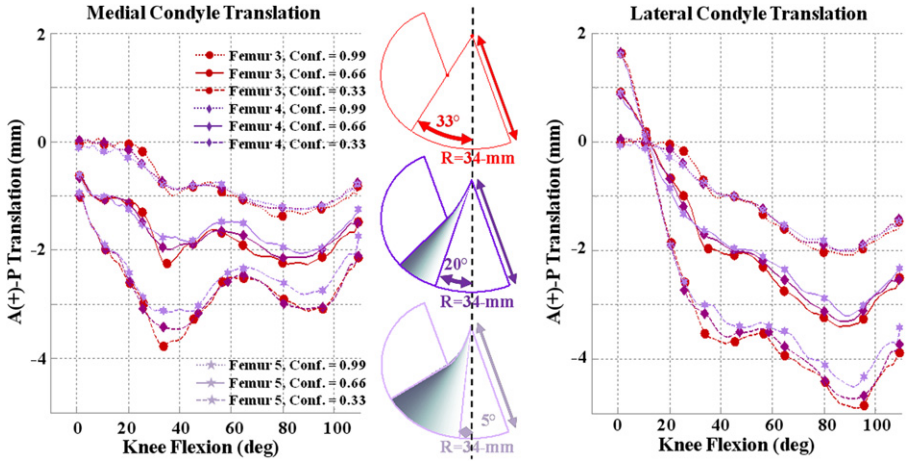

Fig. 4. Predicted A–P motion of the femoral medial condyle (left) and lateral condyle (right) for three femoral components with various transitions from the distal to posterior radii of curvature. One femur had an instantaneous transition, while the other two had gradual transitions over ranges from either 20° to 50° or 5° to 65° flexion.

attenuated the overall magnitude of the paradoxical anterior slide by reducing the initial posterior femoral translation (Fig. 4). The anterior slide of the medial condyle was reduced by 0.3-mm (21%) for the least conforming insert and by 0.16-mm (68%) for the most conforming insert. Increasing the flexion range over which the gradual radius reduction occurred decreased the magnitude of the anterior slide for the least conforming insert, but had minimal influence on the more conforming designs. Incorporating a sudden increase in radius (Femurs 7 and 8) at 65° flexion initiated increased rollback of the medial and lateral condyles in deeper flexion (Fig. 5). The amount of femoral rollback after engagement of the increased radius was greatest for the least conforming inserts.

3.2. Model verification

Low point condylar kinematics measured experimentally in the KKS for the traditional Sigma knee system consistently demonstrated a sudden anterior slide between 30° and 40° flexion; the medial condyle, which had experienced minimal movement from the dwell point in early flexion, shifted anteriorly upon articulation with the sudden transition from distal to posterior radii by an average of 3.1-mm. Meanwhile, the lateral condyle, which had demonstrated continuous posterior motion in early flexion, remained in an approximately static A–P position upon articulation with the posterior radius (Fig. 6). The mean of the experimentally measured condylar kinematics showed good agreement with the model-predicted kinematics for the same implant, with root-mean-square (RMS) differences of 1.3-mm and 0.8-mm for the medial and lateral condyle, respectively.

The experimentally measured kinematics with the Attune knee system, incorporating a gradually reducing radius and a "brake" radius beyond 65° flexion, consistently attenuated the paradoxical anterior slide of the medial condyle by an average of 2.5-mm. Although not statistically different, the experimental kinematics showed increased femoral rollback beyond 65° flexion with the Attune knee system compared to the traditional geometry. The experimentally measured kinematics for the Attune knee system also showed excellent agreement with the model predictions, with RMS differences of 0.5-mm and 1.2-mm for the medial and lateral condyles, respectively.

Calculation of the instantaneous helical axis of rotation highlighted the relationship between anterior slide of the femoral condyles and an abrupt transition in the S–I position of the helical axis from 40-mm to 29-mm between 30° and 40° flexion for the Sigma knee system (Figs. 7 and 8). In comparison, the Attune knee system demonstrated a smoother change in S–I position of the helical axis during flexion (Fig. 8).

4. Discussion

Kinematic behavior after TKA plays a critical role in the overall performance of the implant design and success of the procedure. The results of both the computational evaluation of prototype TKA geometries and the subsequent experimental verification using traditional and contemporary TKA designs demonstrated that the sudden reduction in the radii-of-curvature of femoral condyle was the underlying cause of clinically observed paradoxical anterior femoral translation in mid-flexion. The results also demonstrated that the inverse relationship was true; moving abruptly from a smaller to a larger radius of curvature caused a posterior translation of the femur to occur. While the shape of the femur instigated the motions, the magnitudes of the condylar translations were controlled by the conformity level of the corresponding tibial insert. Utilizing these relationships, condylar kinematics during a DKB could be controlled by fine-tuning transitions between articulating radii of the femur and the conformity level of the tibial insert.

One way to interpret these results is through evaluating the relationship between femoral shape and knee conformity. For example, a dual-radius TKA design with a fully conforming insert against a broad distal radius will have an instantaneous drop in conformity, and thus stability, once the articulation moves from the distal radius onto the posterior radius. Although the design modifications to the femoral articular surface in this study were subtle, utilizing a gradually reducing radius attenuated any sudden reductions in the stability of the joint associated with changes in conformity level.

It remains unclear whether the kinematic variations due to patient factors and surgical technique outweigh the influence of implant design. Recent work by Fitzpatrick et al. (2012) has shown that patient factors are the dominant driver of knee kinematics in extension, but that design factors play a larger role in deeper knee flexion. Furthermore, considerable variation remained in the current experimental analysis despite utilizing consistent implant geometries and externally applied boundary conditions. Despite the variation associated with the subject's soft tissue and implant alignment, in a subject by subject comparison, exchanging the dual radius implant for the gradually reducing radius consistently attenuated the observed paradoxical anterior slide. This is evidence that implant design factors will consistently influence knee kinematics, despite surgical and patient variability.

There are a number of limitations associated with this study. The experimental simulator has mechanical restrictions in its ability to physiologically recreate loading at the knee. In particular, contributions from the multiple heads of the quadriceps muscles in vivo may cause the resultant loading vector applied through the quadriceps tendon to change through the flexion cycle, but in the experimental and computational simulations the

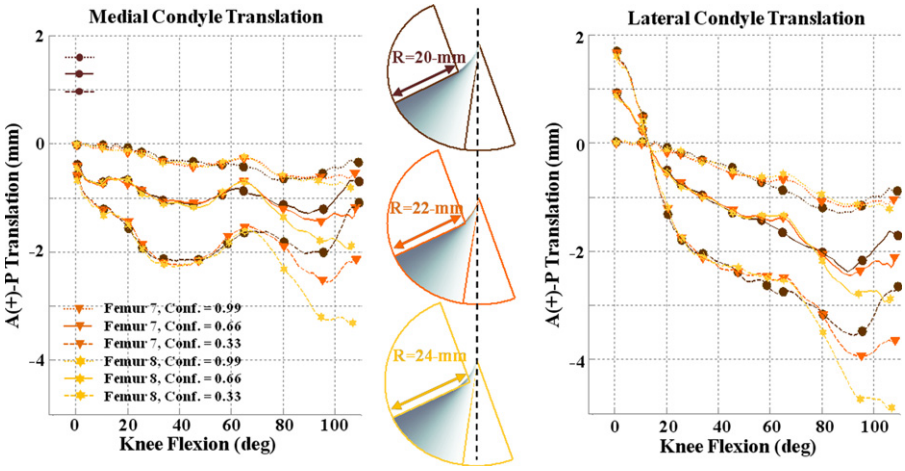

Fig. 5. Predicted A–P motion of the femoral medial condyle (left) and lateral condyle (right) for three femoral components with different levels of "brake" radius. The first design had no sudden increase in radius at 65° flexion while the other two had either a 2-mm or a 4-mm increase.

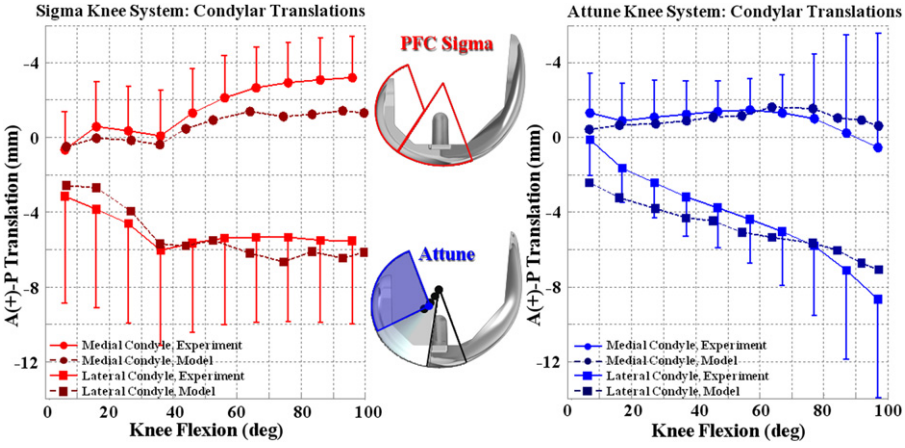

Fig. 6. A–P motion of the femur low point with respect to the tibial insert for the dual-radius design, with abrupt change in A–P motion during the transition from distal to posterior radii (approximately 35°) (left), and for the continuously varying radius design (right).

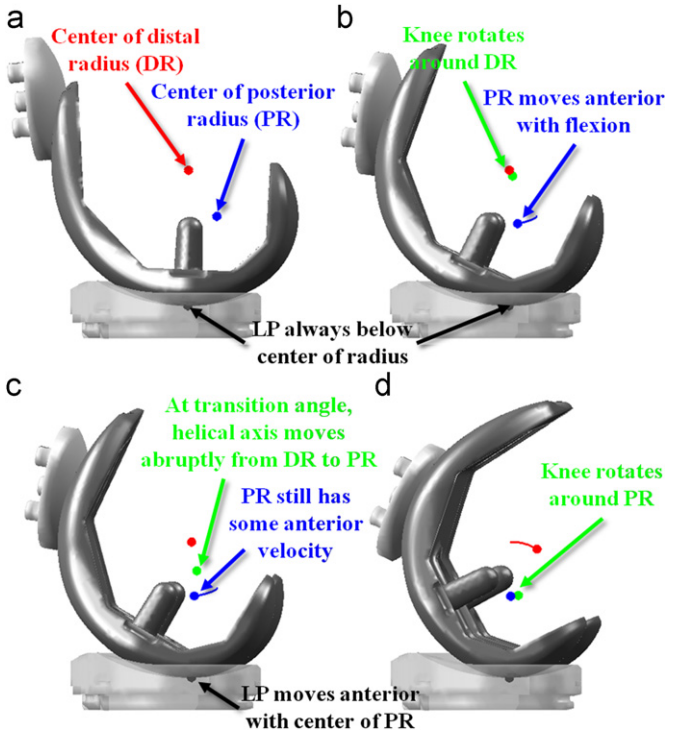

Fig. 7. Motion of the center of the medial distal radius (red), posterior radius (blue), helical axis (green) and medial lowest point (black) for the discrete, multi-radius design, showing abrupt change in position of the instantaneous helical axis during flexion.

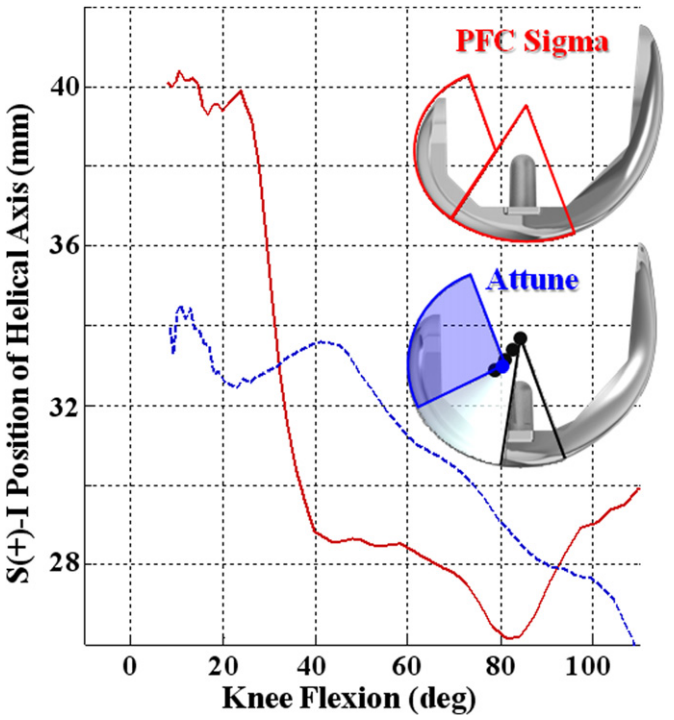

Fig. 8. Superior–inferior position of the instantaneous helical axis during flexion for the dual-radius design (red) and for the gradually reducing radius (blue) designs.

quadriceps mechanism is loaded along a single line of action fixed parallel to the long axis of the femur. In addition, limitations in the strength of the quadriceps tendon restrict the amount of compressive load applied at the hip, such that the tibio-femoral compressive loads in the experiment are lower than are experienced in vivo. Finally, the soft-tissue representation in the current model was composed of mechanical properties and attachment sites tuned to represent a single subject. Each of these factors influenced the overall tibio-femoral kinematics and variation in these boundary conditions may change patterns of the observed kinematics. However, all geometric variations of the implant geometry in both the experiment and computational model were evaluated under identical boundary conditions, so changes in the observed kinematics were contributed solely to the differences in articulating geometry. Future work will assess the behavior of these various implants under more physiological loading conditions and under the variation expected under in vivo use.

Overall, the computational and experimental approach described in this study was effective in identifying the relationship between TKR implant geometry and clinical kinematic observations, enabling design changes to address paradoxical motion. The computational model demonstrated its sensitivity by differentiating changes in kinematic patterns due to subtle changes in implant design, and will subsequently be applied to investigate a host of other design issues including minimizing insert stress and optimizing insert wear behavior.

Conflict of interest statement

One of the authors (CWC) is an employee of DePuy, a Johnson and Johnson company, and one of the authors (PJR) is a consultant to DePuy, a Johnson and Johnson company.

Acknowledgments

The authors would like to thank John Williams and Said Gomaa for their contributions to the computational modeling work motivating this study.

This study was supported in part by DePuy, a Johnson & Johnson company.

References

Amis, A.A., Gupte, C.M., Bull, A.M., Edwards, A., 2006. Anatomy of the posterior cruciate ligament and the meniscofemoral ligaments. Knee Surgery Sports Traumatology Arthroplasty 14 257–6.

Baldwin, M.A., Clary, C.W., Fitzpatrick, C.K., Deacy, J.S., Maletsky, L.P., Rullkoetter, P.J., 2012. Dynamic finite element knee simulation for evaluation of knee replacement mechanics. Journal of Biomechanics 45, 474–483.

Banks, S.A., Harman, M.K., Bellemans, J., Hodge, W.A., 2003a. Making sense of knee arthroplasty kinematics: news you can use. Journal of Bone and Joint Surgery (American) 85-A, 64–72.

Banks, S., Bellemans, J., Nozaki, H., Whiteside, L.A., Harman, M., Hodge, W.A., 2003b. Knee motions during maximum flexion in fixed and mobile-bearing arthroplasties. Clinical Orthopedics and Related Research 410, 131–138.

Banks, S.A., Hodge, W.A., 2004a. Design and activity dependence of kinematics in fixed and mobile-bearing knee arthroplasties. Journal of Arthroplasty 19, 809–816.

Banks, S.A., Hodge, W.A., 2004b. Implant design affects knee arthroplasty kinematics during stair-stepping. Clinical Orthopedics and Related Research 426, 187–193.

Blunn, G.W., Walker, P.S., Joshi, A., Hardinge, K., 1991. The dominance of cyclic sliding in producing wear in total knee replacements. Clinical Orthopedics and Related Research 273, 253–260.

Delport, H.P., Banks, S.A., De Schepper, J., Bellemans, J., 2006. A kinematic comparison of fixed- and mobile-bearing knee replacements. Journal of Bone and Joint Research (British) 88, 1016–1021.

Dennis, D.A., Komistek, R.D., Colwell Jr, C.E., Ranawat, C.S., Scott, R.D., Thornhill, T.S., Lapp, M.A., 1998. In vivo anteroposterior femorotibial translation of total knee arthroplasty: a multicenter analysis. Clinical Orthopedics and Related Research 356, 47–57.

Dennis, D.A., Komistek, R.D., Mahfouz, M.R., Haas, B.D., Stiehl, J.B., 2003a. Multicenter determination of in vivo kinematics after total knee arthroplasty. Clinical Orthopedics and Related Research 416, 37–57.

Dennis, D.A., Komistek, R.D., Mahfouz, M.R., 2003b. In vivo fluoroscopic analysis of fixed-bearing total knee replacements. Clinical Orthopedics and Related Research 410, 114–130.

Godest, A.C., Beaugonin, M., Haug, E., Taylor, M., Gregson, P.J., 2002. Simulation of a knee joint replacement during a gait cycle using explicit finite element analysis. Journal of Biomechanics 35 (2), 267–275.

Grood, E.S., Suntay, W.J., 1983. A joint coordinate system for the clinical description of three-dimensional motions: application to the knee. Journal of Biomechanical Engineering 105, 136–144.

Halloran, J.P., Easley, S.K., Patrella, A.J., Rullkoetter, P.J., 2005. Comparison of deformable and elastic foundation finite element simulations for predicting knee replacement mechanics. Journal of Biomechanical Engineering 127, 813–818.

Halloran, J.P., Clary, C.W., Maletsky, L.P., Taylor, M., Patrella, A.J., Rullkoetter, P.J., 2010. Verification of predicted knee replacement kinematics during simulated gait in the Kansas knee simulator. Journal of Biomechanical Engineering 123, 081010.

Harman, M.K., Banks, S.A., Hodge, W.A., 2001. Polyethylene damage and knee kinematics after total knee arthroplasty. Clinical Orthopedics and Related Research 392, 383–393.

Harman, M.K., DesJardins, J., Benson, L., Banks, S.A., LaBerge, M., Hodge, W.A., 2009. Comparison of polyethylene tibial insert damage from in vivo function and in vitro wear simulation. Journal of Orthopedic Research 27, 540–548.

Harner, C.D., Xerogeanes, J.W., Livesay, G.A., Carlin, G.J., Smith, B.A., Kusayama, T., Kashiwaguchi, S., Woo, S.L., 1995. The human posterior cruciate ligament complex: an interdisciplinary study. Ligament morphology and biomechanical evaluation. American Journal of Sports Medicine 23, 736–745.

Fitzpatrick, C.K., Clary, C.W., Laz, P.J., Rullkoetter, P.J., 2012. Relative contributions of design, alignment, and loading variability in knee replacement mechanics. Journal of Orthopedic Research 30 (12), 2015–2024.

Mahoney, O.M., McClung, C.D., dela Rosa, M.A., Schmalzried, T.P., 2002. The effect of total knee arthroplasty design on extensor mechanism function. Journal of Arthroplasty 17, 416–421.

Maletsky, L.P., Hillberry, B.M., 2005. Simulating dynamic activities using a five-axis knee simulator. Journal of Biomechanical Engineering 127, 123–133.

Race, A., Amis, A.A., 1994. The mechanical properties of the two bundles of the human posterior cruciate ligament. Journal of Biomechanics 27, 13–24.

Stäubli, H.U., Schatzmann, L., Brunner, P., Rinćon, L., Nolte, L.P., 1999. Mechanical tensile properties of the quadriceps tendon and patellar ligament in young adults. The American Journal of Sports Medicine 27 (1), 27–34.

Woltring, H.J., Huiskes, R., de Lange, A., Veldpaus, F.E., 1985. Finite centroid and helical axis estimation from noisy landmark measurements in the study of human joint kinematics. Journal of Biomechanics 18, 379–389.